AIAA 79-2055R

Plasma Processes in Inert-Gas Thrusters

Harold R. Kaufman* and Raymond S. Robinson†
Colorado State University, Fort Collins, Colo.

A model has been developed to describe electron diffusion across a magnetic field that is driven by both density and potential gradients, with Bohm diffusion used to predict the diffusion rate. This model has applications to conduction across magnetic fields inside a discharge chamber, as well as through a magnetic baffle region used to isolate a hollow cathode from the main chamber. Doubly charged ions constitute a significant lifetime limiter for inert-gas ion thrusters. From an existing model for double ion production, correlations have been developed that may be used without experimental data to predict double ion densities for the design of new, and especially larger ion thrusters.

Introduction

INERT-gas thrusters, particularly with large diameters, have continued to be of interest for space propulsion applications. Inert gases are free of some of the practical difficulties associated with mercury propellant such as vaporization, condensation, or environmental concerns. The use of inert-gas propellants has been associated recently with the development of the mutlipole discharge chamber concept.[1-5] The multipole design tends to decouple ion production in the bulk plasma from the current conduction processes in the fringe magnetic fields near the anodes. This is because the fringe fields occupy a small part of the total discharge chamber volume. This decoupling facilitates the analysis involved in elucidating plasma processes taking place in a multipole thruster. Two plasma processes are treated herein: electron diffusion across magnetic fields and double ion production in inert-gas thrusters.

Density-Gradient Driven Electron Diffusion

The electron current to a discharge-chamber anode can be limited by the diffusion of electrons through the magnetic field above the anode. This condition can be thought of as either an anode area limitation or a limitation on current (or current density) to that anode. The current density approach is more convenient for derivation of the effect, while considering an area effect appears to be more useful for discussing experimental performance. The Bohm electron diffusion is discussed primarily in connection with the multipole magnetic field. The effect, though, appears to be involved wherever electrons must cross magnetic field lines to reach a discharge-chamber anode. In addition, electron diffusion across the magnetic baffle region separating a hollow cathode from the main thruster discharge can be studied with the same techniques used to describe anode current collection.

Before presenting the theory of this effect, it should be emphasized that the current collection area involved may, or may not, be a physical area. The electron mobility along magnetic field lines is much greater than the mobility across field lines. The effective area is, therefore, that area from which electrons can be drained from the discharge plasma by traveling along field lines to be collected.

Electrons emitted from the cathode, together with electrons liberated in the ionization process, must diffuse to the anodes to sustain a discharge. In doing so, the electrons must cross magnetic fields sufficient to contain electrons of primary energy. The basic equation for electron diffusion in the presence of potential and density gradients is

$$\Gamma = \mu n_e \nabla V - D \nabla n_e \tag{1}$$

where Γ represents the particle flux of electrons, n_e is the electron number density, and μ and D are the electron mobility and diffusion coefficients, respectively. The mobility and diffusion coefficients are connected by the Einstein relation[6]

$$\mu = eD/kT_e \tag{2}$$

where e is the absolute magnitude of the electronic charge, k is Boltzmann's constant, and T_e is the electron temperature. Experimental measurements of electron diffusion across a magnetic field usually correspond to much larger diffusion coefficients than would be expected classically with the larger values attributed to "anomalous" or "turbulent" diffusion. A simple and well-known semiempirical approach to turbulent electron diffusion was given by Bohm.[7] The Bohm diffusion coefficient given in later publications[8,9] has a slightly different numerical coefficient than originally proposed by Bohm and is, in a magnetic induction B,

$$D_B = kT_e/16eB \tag{3}$$

Bohm diffusion varies as $1/B$, while classical diffusion for the same strong field condition varies as $1/B^2$. In fact, the Bohm value of diffusion is obtained if it is assumed that turbulence increases the effective collision frequency to $\omega/16$, where ω is the electron cyclotron frequency. Despite the apparent simplicity of the Bohm diffusion coefficient, it effectively correlates experimental observations over a wide range of conditions.[9]

It should be noted that the diffusion of interest herein is primarily of Maxwellian electrons. Whether the Coulomb collisions of classical diffusion are considered or the collective collisions of turbulent diffusion, the lower-energy electrons have almost all the collisions, and hence diffuse across a magnetic field preferentially compared to higher-energy primary electrons.

The diffusion condition for anodes that will be considered first is the maximum diffusion that can be obtained without the assistance of a forward electric field, which would result if the anodes were substantially more positive than the discharge-chamber plasma. A reasonable assumption for this limiting condition appears to be zero electric field in the region of interest elose to the anodes of a multipole discharge chamber. This condition of nearly uniform potential in the

Presented as Paper 79-2055 at the Princeton/AIAA/DGLR 14th International Electric Propulsion Conference, Princeton, N.J., Oct. 30-Nov. 1, 1979.

*Professor of Physics. Associate Fellow AIAA.
†Assistant Professor of Physics. Member AIAA.

diffusion region has been observed experimentally.[10] Using the assumption of uniform potential together with the Bohm diffusion coefficient, Eq. (1) can be written in one dimension as

$$\Gamma_x = -D_B \mathrm{d}n_e/\mathrm{d}x \tag{4}$$

where the potential gradient is zero. In terms of current density, this becomes

$$j = eD_B \mathrm{d}n_e/\mathrm{d}x \tag{5}$$

With the substitution of Eq. (3), we find

$$j = \frac{kT_e}{16B}\frac{\mathrm{d}n_e}{\mathrm{d}x} \tag{6}$$

Prior knowledge of the variation of n_e with x is not assumed. Instead, continuity of current flow in the diffusion region is used, which results from the small depth of that region compared to chamber diameter and the small fraction of total ionization therein. Noting also that the electron temperature is also nearly constant in the diffusion region,[10] the constants of Eq. (6) can be collected on the left side to obtain

$$\frac{16j}{kT_e} = \frac{\mathrm{d}n_e}{B\mathrm{d}x} \tag{7}$$

Details of the variation of n_e with x are still not known but the differential expressions can be formally integrated over the diffusion depth to obtain

$$\frac{\mathrm{d}n_e}{B\mathrm{d}x} = \frac{n_e}{\int B\mathrm{d}x} \tag{8}$$

where $\int B\mathrm{d}x$ is the same integral that applies to the containment of high-energy primary electrons.[11] With this substitution, the electron current density becomes

$$j = \frac{kT_e n_e}{16\int B\mathrm{d}x} \tag{9}$$

In calculating this current density, the fringe field area above the anodes is important, while the projected area of the anodes is not. As mentioned earlier, this is because the diffusion coefficient parallel to the magnetic field is so much greater than that normal to the field. The absence of any significant effect of anode projected area has also been established experimentally.[12]

An additional correction can be made for the variation in area normal to the electron current flow j. The magnetic field lines close to the inner anode edges follow paths nearly parallel to the smoothed outer surface of the discharge chamber (see dashed line in Fig. 1). Farther away from the anodes, though, the field lines follow longer, looping paths. This variation in field line length results in a similar variation in area normal to the diffusing electron current. A numerical integration through increments of $\int B\mathrm{d}x$ can be used to correct for this area variation. A numerical expression for the current density is

$$j = \frac{kT_e}{16}\frac{\sum_{i=1}^{N}\Delta n_{e_i}}{\sum_{i=1}^{N}(\Delta\int B\mathrm{d}x)_i d/l_{B_i}} \tag{10}$$

where Δn_{e_i} is the increment in electron density required to drive the current j through an increment in magnetic field integral $(\Delta\int B\mathrm{d}x)_i$ with an area dl_{B_i}, where l_{B_i} is the length of the ith field line and d is a unit length. The local current density thus equals j where $dl_{B_i}/d^2 = 1$. Solving Eq. (10) is facilitated if advantage is taken of the analogy with current flow through resistors connected in series. The increment Δn_{e_i} is analogous to the voltage across a resistor, while the resistance is analogous to $(\Delta\int B\mathrm{d}x)_i d/l_{B_i}$. It can be shown then that an effective overall value for l_{B_i}/d is

$$\frac{l_{B\mathrm{eff}}}{d} = \frac{\int B\mathrm{d}x}{\int B[d/l_B(x)]\mathrm{d}x} \tag{11}$$

where the integral is over the region between the anode and the nearly field-free main volume of the discharge chamber. An appropriate expression for the multipole field is[11]

$$B = B_{\max}\exp[-1.5(x/d+1/2)^2] \tag{12}$$

where x is indicated in Fig. 1. Assuming parabolic arc paths for field lines between the ends of pole pieces, it can be found by integrating Eq. (11) that the area correction yields a current density expression,

$$j \approx \frac{kT_e n_e}{13\int B\mathrm{d}x} \tag{13}$$

where j is based on the area indicated by the dashed line in Fig. 1. Equation (13), then, can be used to find the maximum electron current that will diffuse to the anodes without causing the anodes to become more positive than the discharge-chamber plasma. In view of the relatively small difference between Eqs. (9) and (13), a more accurate correction for the area effect does not appear necessary. Also, a separate correction for corner pole pieces, which have a slightly different variation of B with x, is not required.

Comparison with Experimental Results

The first comparison is with data obtained using the 30-cm multipole discharge chamber (configuration described in Ref. 11). This discharge chamber was operated using a variable number of anodes connected to the positive potential of the discharge supply. The plasma was initially close to anode potential with all the anodes connected. As more anodes were disconnected, the plasma assumed a potential substantially negative of the anodes. This effect is shown in Fig. 2 which was obtained at close to the minimum discharge voltage for each anode configuration; data obtained at discharge voltages about 10 V higher exhibit the same behavior. These operating conditions were determined by operating at a constant

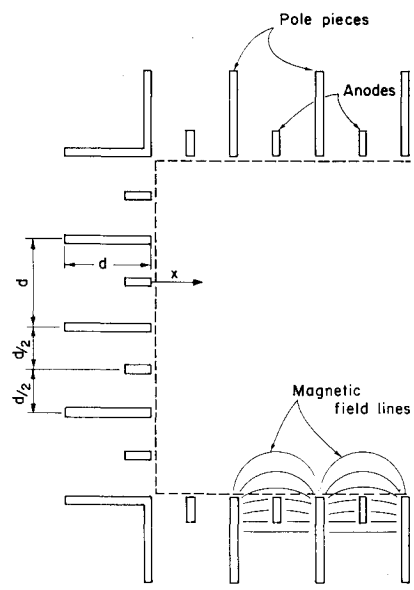

Fig. 1 Multipole discharge chamber. Dashed line shows assumed outer surface of discharge chamber.

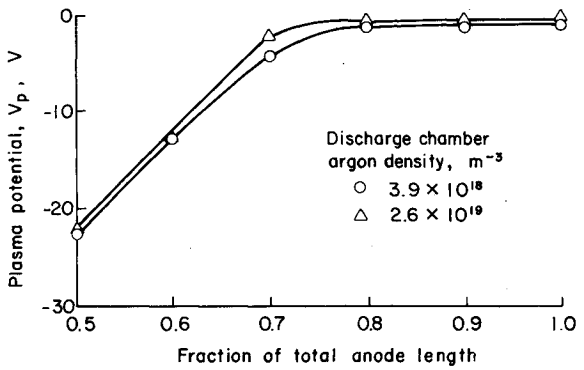

Fig. 2 Plasma potential as a function of anode configuration near the minimum discharge voltage.

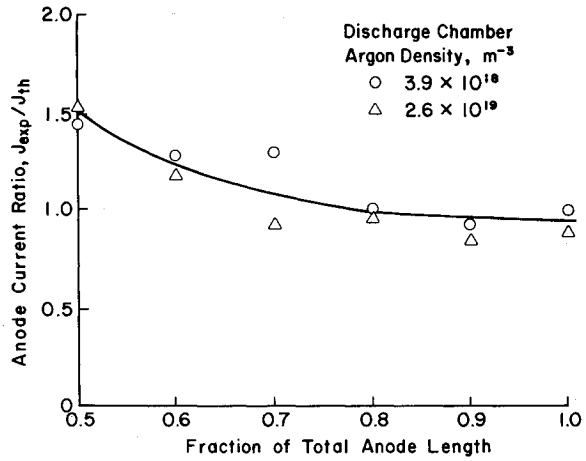

Fig. 3 Experimental-to-theoretical anode current ratios.

discharge current and decreasing discharge voltage. The two propellant densities shown in Fig. 2 cover the usual range of interest for thruster operation. When the effective anode area (proportional to active anode length) is reduced below an approximate critical value, the plasma potential apparently must become increasingly negative of the anodes to maintain the desired electron current to the anodes. Because electron diffusion can result from both potential and density gradients, the added contribution of the potential gradient is the amount required to compensate for the reduced anode area. This contribution is treated later.

Theoretical electron currents to the anodes were calculated using Eq. (13), the effective anode area for the active anodes, and plasma properties from a centrally located Langmuir probe. The experimental anode currents were assumed to be the sums of discharge (emission) and beam currents. The ratios of experimental-to-theoretical anode currents were then plotted in Fig. 3. The trends appear clear. The anode current ratio, J_{exp}/J_{th}, becomes greater than unity at close to the anode fraction where the plasma becomes negative of the anodes. The agreement between J_{exp} and J_{th} shown in Fig. 3 for electron diffusion without assistance from a potential gradient is good, indicating that the physical process is being appropriately modeled in this regime.

Operation with a plasma significantly negative of the anodes is observed to be marginally stable, or even unstable. The data of Figs. 2 and 3 were obtained by using rheostats to gradually disconnect anodes, thereby minimizing switching transients. Without these rheostats, switching of anodes without extinguishing the discharge was reliable only above ~70% of total anode length.[11] That is, it was reliable only at anode lengths where the plasma was not significantly negative of the anodes.

Potential- and Density-Gradient Driven Diffusion

Certain aspects of thruster operation involve strong potential gradients that could substantially enhance the electron diffusion. A general approach to electron diffusion across magnetic fields, which includes effects of both potential and density gradients, is therefore of interest. One such aspect is the diffusion of electrons through a magnetic baffle orifice to the discharge chamber. Yet another is the possible use of anodes more positive than the discharge plasma to provide electrostatic containment of the ions produced, thereby lowering the discharge losses. The data shown in Fig. 2 were adequately described by density-gradient driven diffusion only down to the operating condition where the plasma remained positive of the anodes; to understand the remainder of the experimental data, it is necessary to introduce potential gradients.

The basic relation governing electron diffusion in the presence of both potential and density gradients was given in Eq. (1). The flux rate of Eq. (1) can be multiplied by electron charge to obtain a current density. Also, the usual diffusion problem can be represented as a one-dimensional scalar equation. With the substitutions of Eqs. (2) and (3), the diffusion current density becomes

$$j = \frac{kT_e}{16B}\frac{dn_e}{dx} - \frac{en_e}{16B}\frac{dV}{dx} \tag{14}$$

The volume under consideration is small, so that electron production (through electron-atom impacts) is small and can be ignored. Also, the current density is approximately constant. Using these assumptions,

$$kT_e dn_e - en_e dV = 16jB dx \tag{15}$$

Integrating both sides over the diffusion depth,

$$k\int T_e dn_e - e\int n_e dV = 16j\int B dx \tag{16}$$

and solving for the current density, we find

$$j = (k\int T_e dn - e\int n dV)/16\int B dx \tag{17}$$

It has been shown previously [Eq. (13)] that the factor of 16 should be replaced by 13 when dealing with a multipole design. If both potential and density gradients are present driving the electron diffusion, then most of the potential difference will occur at the lowest density region [see Eq. (14)]. A situation involving both of these gradients will, therefore, tend to have most of the density difference near the source of electrons and most of the potential difference at low density after the electrons have passed through almost all of the density difference.

This problem was examined from a number of different viewpoints using Eqs. (14-17) and similar approaches, but no minimum thickness of the potential gradient region was evident from these equations. But these equations all implicitly assumed continuum processes, and hence did not include the effect of finite orbit size. The realistic lower limit to the potential gradient region was thus decided to be the magnitude of $\int B dx$ such that the entire ΔV would just be sufficient to permit a thermal electron to gain enough energy to escape without a collision.

The first region, dominated by the density gradient, is described by the diffusion equation developed for no potential difference that was derived earlier. This equation can be derived from Eq. (17) by letting T_e be a constant and dV be zero. Integrating from the initial electron density down to zero density, we obtain

$$j = kT_e n_0/13\int B dx \tag{18}$$

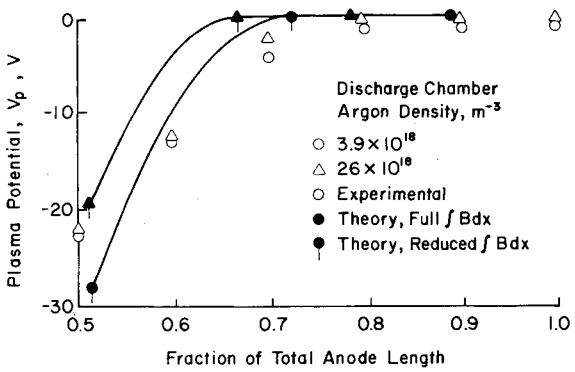

Fig. 4 Comparison between theoretical and experimental plasma potentials as a function of anode configuration.

where n_0 is the bulk plasma density. But it should be remembered that $\int B dx$ is no longer the total integral, but is just that fraction of the integral over which diffusion dominated by the density gradient takes place. To obtain this portion of the integral, the portion that can be crossed by an initially motionless electron due to a potential difference of ΔV must be subtracted from the total integral. This portion was found by analysis to be

$$\Delta \int B dx = (2m\Delta V/e)^{1/2} \tag{19}$$

This result is independent of the variation of V with B and x as long as the ΔV from Eq. (19) is for the portion of $\int B dx$ traversed.[13] The best agreement with experimental data was obtained if an additional increment of $\int B dx$ was also subtracted out due to thermal electrons on the high-density (n_0) side having sufficient energy to penetrate the magnetic field due to their thermal energy alone. This increment is governed by essentially the same equation as that for the penetration of magnetic field by primary electrons,[7]

$$\Delta \int B dx = (8mkT_e/e^2)^{1/2} \tag{20}$$

Subtracting the increments given by Eqs. (19) and (20) from the total value of $\int B dx$ then gives the value to use in Eq. (18).

This method was used to calculate a diffusion current density, hence an anode-area requirement for the experimental data of Fig. 2. Using mean electron temperatures of 4.7 and 3.2 eV and mean electron densities of 1.1×10^{16} and 1.8×10^{16} m^{-3} for the argon neutral densities of 3.9×10^{18} and 2.6×10^{18} m^{-3}, the curves shown in Fig. 4 were calculated. (The temperatures and electron densities given were the average values for the experimental data shown for each neutral density. The anode current averaged about 1.2 A for all the data.) The experimental data are shown by the open symbols. The closed symbols without tails show the current density predicted by Eq. (18) with the full value of $\int B dx$ used. The closed symbols with tails show the same current density, except $\int B dx$ is reduced by the increments of Eqs. (19) and (20). The agreement between theory and experiment is excellent over the entire range of operating conditions.

Applications

As mentioned earlier in this section, the diffusion theory presented appears to be applicable wherever electrons must cross magnetic field lines to reach a discharge-chamber anode. For example, this theory can be applied to mildly divergent magnetic field thrusters. Because the magnetic field lines of such a thruster do not follow long, looping paths, a constant of 16 should replace the constant of 13 in Eq. (13). With this change, a Maxwellian electron temperature of 5 eV, the atomic weight of mercury, a moderate magnetic field integral of 75×10^{-6} T-m, and a typical anode-to-beam current ratio of 11, the minimum ratio of anode collection area to screen open area is about 4. For the usual 50% open screen of early thrusters, this ratio translates into a minimum anode that is about twice the total beam area, or expressed somewhat differently, a minimum length-to-diameter ratio of about 0.5 for the discharge chamber. This result is in qualitative agreement with observations of early thrusters, where a length-to-diameter ratio of unity, or slightly less, showed stable operation. Shorter chambers, though, were hard to start and tended to extinguish easily.

The general case of electron diffusion across magnetic fields also includes diffusion through a baffle gap.[14] This diffusion model is also applicable to general performance trends. For example, the minimum permissible discharge voltage tends to increase as neutral pressure in the discharge chamber is decreased. It is also known that, in most operating ranges of interest, the discharge losses tend to increase as neutral density is decreased. This increase would result in an increase in required anode current at constant discharge voltage, which, in itself, would result in an increased requirement for anode area. If this increased anode area is not available, then the minimum discharge voltage increases until the anode current becomes consistent with the anode area available.

As another example of performance trends, operation with lighter gases has been observed to result in more difficulty in maintaining a discharge, usually with higher minimum discharge voltages. It is observed that electron temperature usually increases somewhat with lighter ion masses, but not as rapidly as the mass decreases. The net effect, then, of electron temperature and ion mass changes should be to require more anode area for a lighter gas. This result is consistent with the observed operational problems described above.

The electrostatic containment of ions (to reduce required discharge losses) was proposed by Moore[15] and Ramsey.[16] Although a significant fraction of the anodes were operated substantially positive of the discharge-chamber plasma in the multipole tests described earlier, no decrease in discharge losses was noted. It would appear that the turbulence expected with Bohm diffusion is probably sufficient to scatter a significant number of ions into the anodes and pole pieces despite the average adverse electric field. The advantage of electrostatic containment thus appears to be offset, at least in part, by the effects of plasma turbulence. However, because a positive ion bias was only obtained with a portion of the anodes at a time, no firm conclusions can be drawn from the data presented.

The diffusion model presented here assumes continuous paths (closed loops) for electron drift velocity normal to any applied electric field. For the observed magnitude of Bohm diffusion, this drift velocity is about 16 times the diffusion velocity in the direction of the applied electric field. This means that, in the presence of an electric field near anodes, the electron drift velocity parallel to the anodes is much greater than the diffusion velocity toward the anodes. When the drift velocity path is interrupted, an electric field is produced normal to the original electric field, which greatly increases electron diffusion due to the original electric field. Translated into multipole anode design, interrupted drift paths should increase the desired diffusion of Maxwellian electrons, easing collection area limitations for the anode as well as reducing minimum discharge voltages.

Doubly Charged Ion Production

Doubly charged ions constitute a significant lifetime problem for inert-gas ion thrusters. A theory exists for the prediction of the doubly charged ion production rate,[17,18] but the utility of this theory is limited by the requirement for prior detailed plasma probe data. Double ion production data in a 15-cm multipole thruster is presented by Wilbur and Kaufman.[19] The present work extends this treatment to larger

thrusters and provides correlations useful in the design stage of ion thruster development.

There is a major need for the prediction of the doubly charged ion production rate in the absence of plasma probe data, preferably even in the absence of any experimental data (in the design phase). The requirement for plasma probe data can perhaps be offset by correlations of plasma properties. The correlations of plasma properties could then be used to estimate these properties in the absence of probe data.

It would be simpler, though, to correlate the production of doubly charged ions directly, instead of calculating from the correlated plasma properties. This approach should be more effective for a family of similar discharge chambers, where the operation of different chambers would be expected to have a basic similarity. Multipole chambers constitute such a family, in addition to having very uniform plasmas throughout most of the chamber volumes.

The ratio of doubly to singly charged ion beam currents is related to the ratio of number densities of the corresponding species in the discharge chamber by

$$I^{++}/I^{+} = 2^{3/2} n_{++}/n_{+} \tag{21}$$

The ratio of number densities in the discharge chamber has been described, in turn, by[18]

$$\frac{n_{++}}{n_{+}} = \frac{\Omega_p}{A_p} F_{++} \times \frac{n_p [P_+^{++} + (n_0/n_+) P_0^{+\,+}] + n_m [Q_+^{++} + (n_0/n_+) Q_0^{+\,+}]}{[2T_m (e/m_i)(1 + n_p/n_m)]^{1/2}} \tag{22}$$

where Ω_p/A_p is the ratio of volume to outside area for the primary electron region, n_p is the density of primary electrons, n_m is the density of Maxwellian electrons, n_+ is the singly charged ion density (for $n_{++} \ll n_+$, $n_+ \approx n_p + n_m$), F_{++} is a uniformity factor for doubly charged ions, T_m is the Maxwellian electron temperature, e/m_i is the charge-to-mass ratio for singly charged ions, $P_0^{+\,+}$ and P_+^{++} are the primary electron rate factors for neutral to doubly ionized and singly to doubly ionized, and $Q_0^{+\,+}$ and Q_+^{++} are the Maxwellian electron rate factors for the same two ionization processes. For a multipole chamber, the primary electron region can be treated as the smoothed-off geometrical shape that will just fit inside the anodes, screen grid, and (if any) the cathode pole piece. The rate factors $P_0^{+\,+}$ and P_+^{++} are functions of primary electron energy, while the rate factors $Q_0^{+\,+}$ and Q_+^{++} are functions of Maxwellian electron temperature. The ratio n_0/n_+ in Eq. (22) can be determined from

$$\frac{n_0}{n_+} = \frac{A_p}{\Omega_p} \frac{[T_m (e/m_i)(1 + n_p/n_m)]^{1/2}}{F_{++}[n_p P_0^{+} + n_m Q_0^{+}]} \tag{23}$$

where P_0^{+} and Q_0^{+} are the primary and Maxwellian electron rate factors for neutral to singly ionized processes.

As shown previously,[18,20] production of doubly charged inert-gas ions can be significant from both primary and Maxwellian electrons, and from both the neutral and singly ionized states. The prediction of most interest is for larger thrusters, with larger values of Ω_p/A_p. From Eq. (23), the ratio of n_0/n_+ becomes smaller with increasing Ω_p/A_p. From this trend and Eq. (22), the $P_0^{+\,+}$ and $Q_0^{+\,+}$ processes will become negligible compared to the P_+^{++} and Q_+^{++} processes as Ω_p/A_p increases.[17] A further change that takes place with increasing thruster size is a decrease in Maxwellian electron temperature, T_m.[17,21,22] The major effect of this change is that the Q_+^{++} process becomes less important than the P_+^{++} process. The primary electron density, n_p, should be (for large thrusters) more important than the Maxwellian electron density, n_m. From an overall performance viewpoint, the primary electron density, n_p, is the major unknown. This density can be related to the total singly charged ion production rate, R^+,

$$R^+ = n_0 n_p P_0^{+} \Omega_p \tag{24}$$

where P_0^{+} is the primary electron rate factor for neutral to singly ionized. This production rate can, in turn, be related to the ion beam current. For this approximate derivation, the doubly ionized contribution to the ion beam current can be ignored, giving

$$J_b = eR^+ (A_s/A_p) \tag{25}$$

where the fraction of ions produced that leave in the ion beam is the ratio of screen open area to primary electron region area, A_s/A_p. For correlation purposes, the P_+^{++} can be approximated by

$$P_+^{++} = K(eV_d - \phi_2) \tag{26}$$

where the primary electron energy is the product of electronic charge and discharge voltage, K is a constant, and ϕ_2 is the energy for double ionization. Combining Eqs. (22-26) yields

$$\frac{(I^{++}/I^{+}) J_0 (1 - \eta_u)}{(J_b/A_s) A_0 (eV_d - \phi_2)} = \frac{F_{++} K \bar{v}_0}{2P_0^{+}} \left(\frac{1 + (n_m/n_p) Q_+^{++}/P_+^{++}}{[T_m (e/m_i)(1 + n_p/n_m)]^{1/2}} \right) \tag{27}$$

An estimate of double ion production for large thrusters can be made from Eq. (27). For this theoretical estimate we assume both $(n_m/n_p) Q_+^{++}/P_+^{++}$ and n_p/n_m negligible compared to unity. This modifies Eq. (27) to

$$\frac{(I^{++}/I^{+}) A_s J_0 (1 - \eta_u)}{A_0 J_b (eV_d - \phi_2)} = \frac{F_{++} K \bar{v}_0}{2P_0^{+} (T_m e/m_i)^{1/2}} \tag{28}$$

For F_{++}, the average value of 7 can be used from previous studies with multipole chambers.[16] For K, the value is about 3.0×10^{-15} m^3/eV-s for xenon and about 1.6×10^{-15} m^3/eV-s for argon. For $\bar{v}_0$, the effective neutral temperature can be assumed to be about 600 K. For P_0^{+}, the values are: 1.4×10^{-13} m^3/s for xenon and 9.7×10^{-14} m^3/s for argon. (P_0^{+} does not vary rapidly with primary electron energy in the range of interest, but an electron energy of $\phi_1 + \phi_2$ was used for the preceding values.) For Maxwellian electron temperature, a value of $\phi_1/4$ was assumed. This value is in rough agreement with the 30-cm Maxwellian temperatures observed for mercury and argon propellant.[17,22] Using these values in Eq. (28), we find

$$\frac{(I^{++}/I^{+}) J_0 (1 - \eta_u)}{(J_b/A_s) A_0 (eV_d - \phi_2)} = 0.0157 \text{ (Xe)}, \quad 0.0105 \text{ (Ar)} \tag{29}$$

Dividing both sides by the neutral loss parameter,

$$\frac{(I^{++}/I^{+}) A_p A_s}{J_b (eV_d - \phi_2) \Omega_p} = 0.0157 \left(\frac{J_0 (1 - \eta_u) \Omega_p}{A_0 A_p} \right)^{-1} \text{ (Xe)} \tag{30a}$$

$$\frac{(I^{++}/I^{+}) A_p A_s}{J_b (eV_d - \phi_2) \Omega_p} = 0.0105 \left(\frac{J_0 (1 - \eta_u) \Omega_p}{A_0 A_p} \right)^{-1} \text{ (Ar)} \tag{30b}$$

These equations are plotted in Figs. 5 and 6. The experimental data fall below the theory for both propellants, but come closest at high neutral loss parameters where low Maxwellian temperatures and low values of n_p/n_m would be expected. Increasing the thruster size from the 15-cm size used for data presented herein would be expected to give closer agreement

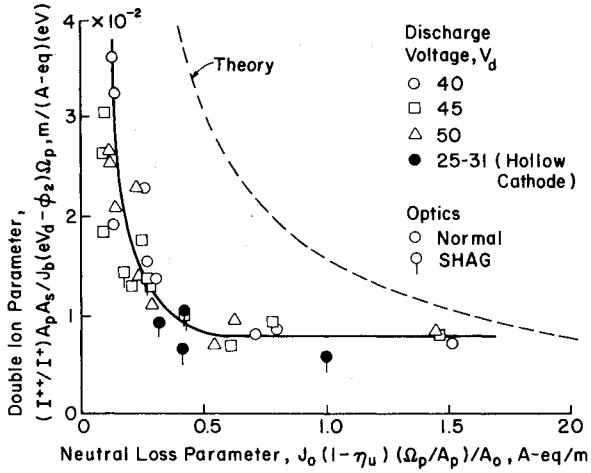

Fig. 5 Double ion correlation for xenon showing comparison with theory for large thrusters.

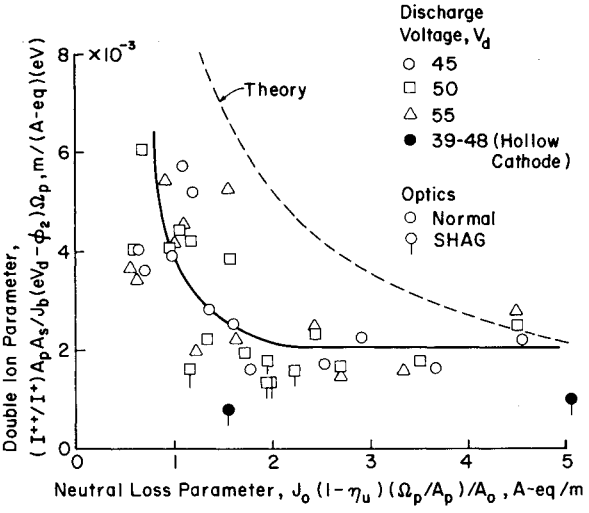

Fig. 6 Double ion correlation for argon, showing comparison with theory for large thrusters.

with the theory. Predictions for thrusters larger than the 15-cm size should, therefore, be between the experimental and theoretical curves.

Some additional double ion data were also included in Figs. 5 and 6. These were some small-hole-accelerator-grid (SHAG) data,[18] and some hollow cathode data.[23] Except for the latter, all the rest of the data were obtained with refractory cathodes. One might expect a lower double ion production with a hollow cathode (other parameters being the same) because some primary electron energy should be lost in the baffle region plasma. This effect does not appear significant for xenon, but may be the cause of the two argon hollow cathode points being lower in Fig. 6. It is probably significant that coupling voltages (cathode to adjacent plasma) are larger for argon than for xenon.

From the data correlations presented in Figs. 5 and 6, the double ion production of a multipole discharge chamber can be predicted from overall performance parameters and geometrical considerations of the discharge chamber and ion optics. The experimental data were all obtained with 15-cm-diam discharge chambers. The theoretical curves in Figs. 5 and 6 were included to indicate the trends that would be expected for much larger thrusters.

Additional data, obtained more recently[24] using a 30-cm argon thruster, are generally in agreement with the 15-cm data of Fig. 6. The only exceptions were data obtained at 60-70-V discharges, where single step double ion production would be expected to be significant, hence violating the assumption of two step double ion production as the dominant process.

Concluding Remarks

A comprehensive theory for electron diffusion across magnetic field lines in the presence of both plasma density and electric potential gradients is presented. The basic diffusion process appears to be anomalous or turbulent in nature, agreeing with the semiempirical Bohm coefficient. Substitution of integral values for differential ones in the current density equation resulted in convenient equations that do not require detailed knowledge of parameter variations within the diffusion region. For the case of diffusion driven by a plasma density gradient alone, the electron temperature, the electron density difference, and the integral of magnetic field ($\int B dx$) are all that are required to calculate the electron current density in the direction of the density gradient.

The solution with both plasma and potential gradients driving the diffusion is somewhat more complicated. Detailed analysis and consideration of physical processes indicated that the combination of both driving gradients could be approximated with a two step process. At the negative side of the diffusion region, the diffusion can be treated as being due to only a gradient in plasma density (equipotential). At the positive side of the region, traversal of the magnetic field is due only to the potential difference and is equivalent to one-fourth of a cyclotron orbit. An additional refinement (usually not important) includes the initial penetration of the magnetic field on the negative side of the diffusion region due to electron thermal energy. The diffusion in the presence of both gradients is then calculated by subtracting that portion of the magnetic field integral that is penetrated due to the potential difference (and also initial thermal energy, if desired), then determining current density from the total density difference and the remaining portion of the magnetic integral.

The predictions of this electron diffusion model are in qualitative and quantitative agreement with a wide range of experimental observations. These observations include discharge-chamber operating limits, diffusion to multipole anodes, and diffusion through a pole-piece baffle gap. This theory should be a highly effective tool in both design and performance analysis.

The theory for double ion production presented herein is not as complete as the electron diffusion theory described above, but it should also be a useful tool for predicting double ion sputter erosion. Starting from a more complete theory that required detailed probe analysis, knowledge of the relative magnitudes of the various physical processes was used to derive approximate equations for large inert-gas thrusters. The double ion production data from 15-cm-diam thrusters was effectively correlated by parametric groupings derived from these equations. Numerical values were also obtained from the equations to indicate the double ion production that would be expected for much larger thrusters. The most pressing need at present appears to be experimental double ion data from larger thrusters. The present theory, though, should be effective for both preliminary estimates and predicting qualitative trends.

Acknowledgment

This work was performed under NASA Grant NSG 3011.

References

[1] Kaufman, H.R., "Experimental Investigation of Argon and Xenon Ion Sources," NASA CR-134845, June 1975.

[2] Isaacson, G.C. and Kaufman, H.R., "15-cm Multipole Gas Ion Thruster," *Journal of Spacecraft and Rockets*, Vol. 14, 1977, pp. 469-473.

[3] Isaacson, G.C., "Multipole Gas Thruster Design," NASA CR-135101, June 1977.

[4] Robinson, R.S. and Kaufman, H.R., "Ion Thruster Technology Applied to a 30-cm Multipole Sputtering Ion Source," *AIAA Journal*, Vol. 15, May 1977, pp. 702-706.

[5] Ramsey, W.D., "12-cm Argon/Xenon Ion Source," *Journal of Spacecraft and Rockets,* Vol. 16, July-Aug. 1979, pp. 252-257.
[6] Chen, F.F., *Introduction to Plasma Physics,* Plenum, New York, 1974, pp. 165-173.
[7] Bohm, D., "Qualitative Description of the Arc Plasma in a Magnetic Field," *The Characteristics of Electrical Discharges in Magnetic Fields,* edited by A. Guthrie and R.K. Wakerling, McGraw-Hill Book Co., New York, 1949, pp. 1-12.
[8] Spitzer, L. Jr., *Physics of Fully Ionized Gases,* 2nd ed., Interscience, New York, 1962, pp. 47-48.
[9] Chen, F.F., *Introduction to Plasma Physics,* Plenum, New York, 1974, p. 169.
[10] Robinson, R.S., "Plasma Probe Measurements in the 30-cm Discharge Chamber," *Industrial Ion Source Technology,* edited by H.R. Kaufman, NASA CR-135353, Nov. 1977, pp. 3-17.
[11] Robinson, R.S., "Thirty cm Ion Source," *Industrial Ion Source Technology,* edited by H.R. Kaufman, NASA CR-135149, Nov. 1976, pp. 1-59.
[12] Isaacson, G.C., "Multipole Gas Thruster Design," NASA CR-135101, June 1977, pp. 45-51.
[13] Robinson, R.S., "Physical Processes in Directed Ion Beam Sputtering," NASA CR-159567, March 1979, Appendix A.
[14] Brophy, J.R. and Wilbur, P.J., "Design Model for the Baffle Aperture Region of a Hollow Cathode Thruster," AIAA Paper 81-0758, April 1981.
[15] Moore, R.D., "Magneto-Electrostatically Contained Plasma Ion Thruster," AIAA Paper 69-260, March 1969.
[16] Ramsey, W.D., "12-cm Magneto-Electrostatic Containment Mercury Ion Thruster Development," *Journal of Spacecraft and Rockets,* Vol. 9, May 1972, pp. 318-321.
[17] Peters, R.R., "Double Ion Production in Mercury Thrusters," NASA CR-135019, April 1976.
[18] Wilbur, P.J., "Inert Gas Thrusters," edited by H.R. Kaufman, NASA CR-135226, July 1977, pp. 46-64.
[19] Wilbur, P.J. and Kaufman, H.R., "Double Ion Production in Argon and Xenon Ion Thrusters," *Journal of Spacecraft and Rockets,* Vol. 16, July-Aug. 1979, pp. 264-267.
[20] Wilbur, P.J. and Kaufman, H.R., "Scaling Relationships for Mercury and Gaseous Propellant Ion Thrusters," AIAA Paper 78-667, April 1978.
[21] Isaacson, G.C., "Multipole Gas Thruster Design," NASA CR-135101, June 1977.
[22] Robinson, R.S., "Industrial Ion Source Technology," NASA CR-135353, Nov. 1977, pp. 3-23.
[23] Rehn, L.A., "Inert Gas Thrusters," edited by H.R. Kaufman, NASA CR-159537, Nov. 1978, pp. 33-49.
[24] Kaufman, H.R. and Robinson, R.S., "Inert Gas Thrusters," NASA CR-165332, Dec. 1980.